Computer Assisted Mechanics and Engineering Sciences, 15: 123–142, 2008.

Essential boundary conditions in meshfree methods via a modified variational principle. Applications to shell computations

Sebastian Skatulla, Carlo Sansour
School of Civil Engineering, The University of Nottingham, University Park Nottingham NG7 2RD, UK

(Received March 10, 2008)

It has been recognized by many authors that the enforcement of the essential boundary conditions is not an easy task, when it comes to *moving least square* (MLS)-based meshfree methods. In particular, the modelling of non-linear problems requires high approximation accuracy in order to obtain a solution. This paper addresses the boundary approximation accuracy of MLS-based meshfree methods and shows more specifically its significance with respect to the imposition of essential boundary conditions by the penalty, the Lagrange multiplier method and their combination which results in a modified variational principle. The later is augmented by a stabilization term which uses individual stabilization parameters determined for each numerical integration point by an iteration procedure.

This methodology is demonstrated on shell deformations in non-linear structural mechanics involving the Green strain tensor and two different hyper-elastic material laws.

Keywords: Meshfree methods; moving least square method; essential boundary conditions; shell analysis

1. Introduction

The last decade witnessed increasing research activity in so-called *meshfree methods*, as these methods can deal especially well with problems characterized by large deformations, changing domain geometry, or necessitate higher order approximation continuity. These are areas, where the more established finite element method (FEM) exhibits shortcomings. Essentially, meshfree methods do not require a rigid background mesh which is beneficial as finite element modelling of large deformation problems usually leads to mesh distortion which makes re-meshing necessary. In most large-scale numerical simulations of physical phenomena however, a high percentage of the overall computational efforts is expended on technical details connected with meshing. These details include, in particular, grid generation, mesh adaptation to domain geometry, element or cell connectivity, grid motion, and separation of mesh cells to model fracture, fragmentation and free surfaces. Moreover, in most computer-aided design work, the generation of an appropriate mesh constitutes, by far, the most costly portion of the computational analysis.

Clearly, meshfree methods have much potential for alleviating some of the difficulties associated with finite element analysis. Prominent examples are the diffuse element method [18], the element-free Galerkin method [4], the reproducing kernel particle method [14], the partition of unity method [17] and the hp-cloud method [10]. In particular, the use of *moving least squares* (MLS) [13] within meshfree methods was found very appealing as it results in a smooth global approximation of the solution function.

However, when applying MLS-based meshfree methods to an elliptic PDE the enforcement of the corresponding essential boundary conditions provides difficulties. The reasons for this are twofold. Firstly, the direct and explicit enforcement of essential boundary conditions, which is the common procedure in FEM, is not available for meshfree methods. This is rooted in the fact that the

approximation functions do not possess the Kronecker-Delta property. Secondly, the boundary areas exhibit a limited particle support, as there is no support from outside the problem domain. In order to ensure the minimum necessary support, the influence zones of those particles adjacent to the boundary have to be larger than within the domain which consequently results in a significantly reduced approximation accuracy at and near the boundary. This fact causes difficulties, if the problem formulation involves boundary integral expressions.

As mentioned before, the traditional boundary collocation method used in FEM can not be applied to MLS-based meshfree methods. Wagner and Liu [24] therefore proposed to modify the meshfree shape function in such a way that they interpolated on particles having essential boundary conditions applied. The Dirichlet boundary conditions could be explicitly imposed on the collocation points, which are the boundary particles, very much as in FEM. This procedure has been called modified boundary collocation method. The solution at the boundary particles was obtained with the highest numerically possible precision which made it numerically very stable.

The procedure appears to be very straightforward as the essential boundary conditions can be directly enforced, after the discrete equation system has been modified. However, the implementation is very involved. Firstly, in order to avoid large scale matrix multiplications those parts of the discrete equation system, which have to be modified, must be determined beforehand. This requires an elaborate algorithm as the boundary particles only interact with certain particles in their vicinity and correspondingly, the majority of the discrete equation system is not affected. Secondly, the coefficient matrix is usually stored in a sparse storage scheme so that only the band structure of it is considered. After the modification of the coefficient matrix some elements of the original matrix which happen to be zero become non-zero in the modified matrix. This fact must be taken into account, when the structure of the sparse storage scheme is initially ascertained.

Another issue is that during the transformation of the discrete equation system the original coefficient matrix and the modified one must be kept allocated at the same time. Thus, already medium size problems can exceed the memory limits of a single workstation.

Furthermore, despite the fact that the boundary condition enforcement is precise at the boundary particles, it is not on the Dirichlet boundary as a whole. This is due to the characteristic of MLS-based meshfree methods that the boundary conditions are literally enforced only on the boundary particles but not between them. In case of the Gauss quadrature however, the integration points are distributed between the boundary particles, where the boundary conditions are not exactly enforced. Whereas the finite element method can fulfill constant essential boundary conditions exactly on the entire Dirichlet boundary, this is not the case for meshfree methods using the modified boundary collocation method. Especially for a curved boundary a sufficiently dense particle distribution on the boundary must be ensured in order to provide an accurate solution on the boundary and consequently for the whole domain.

Using the *penalty method* is probably the easiest way to impose the essential boundary conditions [3, 15]. It results in a banded and positive definite coefficient matrix of the discrete equation system. The boundary enforcement accuracy corresponds to the magnitude of the penalty parameter, which, accordingly, has to be set to a fairly high value. However, the solution is significantly dependent on the value of the penalty parameter considering that the penalizing physically represents the stiffness of fictional springs enforcing the constraints. If the essential boundary conditions affect large parts of boundary, the problem can become unsolvable as the penalty treatment basically replaces parts of the coefficient matrix of the discrete equation system by values of very high magnitude which are not related to the initial formulation which describes the physical state of the body under consideration [7]. Especially in MLS-based meshfree methods the affected parts of the coefficient matrix are much larger than in FEM due to the larger particle support.

An alternative is the *Lagrange multiplier method* which introduces to the problem formulation another unknown field the so-called *Lagrange multipliers* [4, 6, 23]. Even if the implementation of this method is not complicated and a very high boundary condition fulfillment accuracy can be achieved, it has to deal with two main disadvantages. Firstly, the problem size is increased as it contains a further unknown field and secondly, the coefficient matrix of the discrete equation

system is neither positive definite nor banded. This procedure is therefore not suitable for larger problems.

These drawbacks can be partly avoided, if the Lagrange multipliers can be identified with a physical quantity corresponding to constraint reaction resultant. This leads to a modified variational principle [16] which holds the benefit that the coefficient matrix of the discrete equations system is banded. However, the boundary enforcement accuracy is significantly less compared to the original Lagrange multiplier method. The authors mentioned that an increase of the particle distribution near to Dirichlet boundary could enhance the imposition of essential boundary conditions. Nevertheless, the presented examples only consider linear geometry and material, whereas non-linearity requires higher accuracy to achieve a reasonable convergence rate.

The insufficient boundary enforcement accuracy of this kind of modified variational principle can be improved, if a penalty term is added [19]. The stabilized modified variational principle holds the benefit that the coefficient matrix is not as much manipulated as in case of the penalty method, because the penalty term only serves for stabilizing purpose and so the magnitude of the penalty parameter can be set lower than in case of the penalty method. Nevertheless, the stabilization term ensures that the coefficient matrix is not ill-conditioned.

Related to this approach is the so-called *augmented Lagrangian method* [12, 21] which was initially proposed in order to improve the Lagrange multiplier method by avoiding an ill-conditioned discrete equation system and so ensuring a higher convergence rate.

This paper now is organized as follows: After a brief introduction to the moving least square method in Section 2, a modified variational formulation is presented in Section 3. In Section 4 a new technique is proposed which allows to stabilize the modified variational principle introduced in the previous section in a flexible and adaptive way. The last section demonstrates the applicability of our problem formulation on various examples ranging from two-dimensional problem configurations to demanding shell structures. Further, the impact of non-linearity in geometry as well as in material is studied with regard to the boundary condition imposition accuracy and numerical stability.

2. Moving least square method

In the *moving least square method* [13] an approximation for a solution is constructed based on a given set of particles. In the following we outline the MLS method briefly.

Let us consider any function $u(x)$ defined over the field Ω. A possible approximation for $u(x)$ is defined by a complete polynomial $\mathbf{P}(x)$ and its non-constant coefficients $\mathbf{a}(x)$,

$$u^h(x) = \mathbf{P}(x) \cdot \mathbf{a}(x), \tag{1}$$

where scalar products of vectors are denoted by a dot. The basis polynomial is chosen to be of second order and of the Pascal type. To each particle, a so-called weight function Φ with compact support is attached. A parameter ϱ defines the so-called *influence radius* of Φ. The sum of all particles with coordinates x_I, that support the point x, constitute the set Λ. With the help of this set a weighted least square fit in the vicinity of a point x can be constructed according to

$$J(\mathbf{a}(x)) := \sum_{I \in \Lambda} \left[\mathbf{P}(x_I) \cdot \mathbf{a}(x) - u(x_I)\right]^2 \Phi\left(\frac{x - x_I}{\varrho}\right). \tag{2}$$

In our case function Φ is taken to be a quartic C^3-continuous spline.

The unknown coefficients $\mathbf{a}(x)$ can be determined by minimizing the functional J with respect to $\mathbf{a}(x)$. Then the substitution of the coefficients $\mathbf{a}(x)$ in Eq. (1) provides the approximation of $u(x)$ as follows,

$$u^h(x) = \mathbf{P}(x) \cdot \mathbf{M}^{-1}(x) \sum_{I \in \Lambda} \mathbf{P}(x_I)\, \Phi\left(\frac{x - x_I}{\varrho}\right) u_I, \tag{3}$$

where $\mathbf{M}(x)$ is the so-called *moment matrix* of the weight function Φ,

$$\mathbf{M}(x) = \sum_{I=\Lambda} \mathbf{P}(x_I)\,\mathbf{P}(x_I)\,\Phi\left(\frac{x - x_I}{\varrho}\right), \tag{4}$$

and u_I are the so-called particle parameters. Lancaster and Salkauskas outlined in [13] that if the basis polynomial $\mathbf{P} \in C^m(\Omega)$ and the weight function $\Phi \in C^l(\Omega)$, then we have for smoothness of the global approximation $u^h(x) \in C^k(\Omega)$, where $k = \min\{m, l\}$. In this work a complete polynomial of second order is utilized so that the MLS approximation possesses C^2 continuity everywhere.

The choice for the particle influence radius ϱ is critical, as it effects stability and accuracy of the method. In this work the influence radius is determined automatically by a computer algorithm. Essentially, each particle has assigned individual radii for each positive and negative co-ordinate direction. Since the numerical integration resorts to a finite element background mesh, this mesh is also utilized to ensure a suitable particle influence radius setting. That is, each particle has to support those particles which are connected to the same element, we call direct neighbour particles. Additionally, the direct neighbour particles of the former are included as well which we call indirect neighbour particles. This method is numerically very efficient, because no search algorithm is needed which has to account for all particles in the domain. It also allows for high adaptivity and flexibility, when it comes irregular particle distributions.

3. A MODIFIED VARIATIONAL PRINCIPLE

Let us consider a non-linear boundary value problem on domain $\mathcal{B}$ with boundary $\partial\mathcal{B}$. Dirichlet boundary conditions are prescribed on $\partial\mathcal{B}_D \subset \partial\mathcal{B}$ and Neumann boundary conditions are prescribed on $\partial\mathcal{B}_N = \partial\mathcal{B} \setminus \partial\mathcal{B}_D$.

Now let $\mathbf{F}(\mathbf{u}) = \mathbf{1} + \mathrm{Grad}\,\mathbf{u}$ be the deformation gradient and $\mathbf{E}(\mathbf{u}) = \frac{1}{2}(\mathbf{F}^T\mathbf{F} - \mathbf{1})$ the Green strain tensor. Assume a hyperelastic material behaviour and let $\psi(\mathbf{E})$ define the stored energy function per unit volume. Further, let $\mathcal{W}_{ext}$ define the external potential as follows,

$$\mathcal{W}_{ext}(\mathbf{u}) = -\int_{\mathcal{B}} \mathbf{b}\cdot\mathbf{u}\,\mathrm{d}V - \int_{\partial\mathcal{B}_N} \hat{\mathbf{t}}\cdot\mathbf{u}\,\mathrm{d}A\,, \tag{5}$$

where $\mathbf{b}$ is the body force and $\hat{\mathbf{t}}$ is the external traction vector prescribed on $\mathcal{B}_N$. $\mathrm{d}V$ is a volume element of domain $\mathcal{B}$, whereas $\mathrm{d}A$ is a surface element of its corresponding boundary $\partial\mathcal{B}$. We start from the following variational statement,

$$\delta\Pi(\mathbf{u}) = \int_{\mathcal{B}} \mathbf{S} : \delta\mathbf{E}\,\mathrm{d}V - \int_{\mathcal{B}} \mathbf{b}\cdot\delta\mathbf{u}\,\mathrm{d}V - \int_{\partial\mathcal{B}_N} \hat{\mathbf{t}}\cdot\delta\mathbf{u}\,\mathrm{d}A = 0\,, \tag{6}$$

where $\mathbf{S}$ is the second Piola–Kirchhoff stress tensor given by

$$\mathbf{S}(\mathbf{u}) = \frac{\partial\psi(\mathbf{E})}{\partial\mathbf{E}}\,. \tag{7}$$

The double dot operator (:) denotes the scalar product of tensors. The above functional corresponds to the following Euler–Lagrange field equations,

$$\mathrm{Div}(\mathbf{FS}) + \mathbf{b} = \mathbf{0} \quad \text{in } \mathcal{B}, \qquad \mathbf{FSn} - \hat{\mathbf{t}} = \mathbf{0} \quad \text{on } \partial\mathcal{B}_N\,, \tag{8}$$

where $\mathbf{n}$ defines the normal vector at the boundary. These field equations are supplemented by essential boundary conditions, the so-called Dirichlet boundary conditions

$$\mathbf{u} = \hat{\mathbf{u}} \quad \text{on } \partial\mathcal{B}_D\,. \tag{9}$$

To incorporate the essential boundary conditions in the functional itself, that is to enforce these conditions as Euler–Lagrange equation, the functional (6) is modified in the following way,

$$\delta \Pi(\mathbf{u}) = \int_{\mathcal{B}} \mathbf{S} : \delta \mathbf{E} \, \mathrm{d}V + \int_{\partial \mathcal{B}_D} \delta \left(\boldsymbol{\lambda} \cdot (\mathbf{u} - \hat{\mathbf{u}}) \right) \mathrm{d}A - \int_{\mathcal{B}} \mathbf{b} \cdot \delta \mathbf{u} \, \mathrm{d}V - \int_{\partial \mathcal{B}_N} \hat{\mathbf{t}} \cdot \delta \mathbf{u} \, \mathrm{d}A = 0 \,. \tag{10}$$

Making use of *Gauss divergence theorem* this formulation is transferred back to its strong form which is the integral form of the Euler–Lagrange equations,

$$\begin{aligned} \delta \Pi(\mathbf{u}) = & - \int_{\mathcal{B}} \mathrm{Div}(\mathbf{FS}) \cdot \delta \mathbf{u} \, \mathrm{d}V + \int_{\partial \mathcal{B}} \mathbf{FSn} \cdot \delta \mathbf{u} \, \mathrm{d}A + \int_{\partial \mathcal{B}_D} \boldsymbol{\lambda} \cdot \delta \mathbf{u} \, \mathrm{d}A \\ & + \int_{\partial \mathcal{B}_D} \delta \boldsymbol{\lambda} \cdot (\mathbf{u} - \hat{\mathbf{u}}) \, \mathrm{d}A - \int_{\mathcal{B}} \mathbf{b} \cdot \delta \mathbf{u} \, \mathrm{d}V - \int_{\partial \mathcal{B}_N} \hat{\mathbf{t}} \cdot \delta \mathbf{u} \, \mathrm{d}A = 0 \,. \end{aligned} \tag{11}$$

Since this integral equation must be valid for any arbitrary $\delta \mathbf{u}$, we can extract the Euler–Lagrange equations (8) and identify the Lagrange multipliers as $\boldsymbol{\lambda} = -\mathbf{FSn}$ on $\partial \mathcal{B}_D$. Note that the second term in Eq. (11) is an integral expression over the entire boundary $\partial \mathcal{B}$. The final problem statement takes the following form,

$$\begin{aligned} \delta \Pi(\mathbf{u}) = & \int_{\mathcal{B}} \mathbf{S} : \delta \mathbf{E} \, \mathrm{d}V - \int_{\partial \mathcal{B}_D} \mathbf{FSn} \cdot \delta \mathbf{u} \, \mathrm{d}A - \int_{\partial \mathcal{B}_D} \delta(\mathbf{FSn}) \cdot (\mathbf{u} - \hat{\mathbf{u}}) \, \mathrm{d}A \\ & - \int_{\mathcal{B}} \mathbf{b} \cdot \delta \mathbf{u} \, \mathrm{d}V - \int_{\partial \mathcal{B}_N} \hat{\mathbf{t}} \cdot \delta \mathbf{u} \, \mathrm{d}A = 0 \,. \end{aligned} \tag{12}$$

4. A STABILIZED MODIFIED VARIATIONAL PRINCIPLE

The modified variational principle outlined in the previous section heavily relies on the accurate evaluation of the boundary integral expression. This is due to the fact that the definition of the Lagrange multipliers $\boldsymbol{\lambda} = -\mathbf{FSn}$ relates to *Gauss's divergence theorem* which states the equivalence of a volume and a surface integral expression. This equivalence however, is not given anymore, if the numerical accuracy is substantially lacking. Consequently, the essential boundary condition fulfillment can not be ensured anymore which also affects the solution for the entire problem domain. Breitkopf and his co-workers [5] as well as De and Bathe [8] noted that MLS-based formulations can not be as accurately integrated due to the non-polynomial character of the meshfree approximation function. Dolbow and Belytschko also made the misalignment between particle support zones and integration cells responsible for the reduced numerical integration accuracy [9]. Especially the spherical particle influence zone was said to be disadvantageous. Therefore they proposed a so-called bounding box technique to match particle support and background mesh and so to improve the performance of the integration.

However, it can also be found that the meshfree approximation quality close to the boundary is significantly worse than within the domain. This is clear, as the particle support of the boundary area is less than that of the domain interior and consequently, the influence zones of those particles close the boundary must be chosen larger than within the domain in order to compensate this lack of support. Larger particle influence zone though, result in a solution approximation which is less local and therefore less accurate. Consequently, the mathematical equivalence of volume and surface integral expressions is disturbed and so, the solution behaviour can become unstable.

An approach to stabilize the modified variational principle introduced in Section 3 is to incorporate an additional stabilization or penalty term, the purpose of which is to balance out the lacking

boundary approximation and boundary condition enforcement accuracy. The problem formulation introduced in the previous section is then extended as follows,

$$\delta\Pi(\mathbf{u}) = \int_{\mathcal{B}} \mathbf{S} : \delta\mathbf{E}\,\mathrm{d}V - \int_{\partial\mathcal{B}_D} \mathbf{FSn}\cdot\delta\mathbf{u}\,\mathrm{d}A - \int_{\partial\mathcal{B}_D} \delta(\mathbf{FSn})\cdot(\mathbf{u}-\hat{\mathbf{u}})\,\mathrm{d}A$$
$$+\beta\int_{\partial\mathcal{B}_D}(\mathbf{u}-\hat{\mathbf{u}})\cdot\delta\mathbf{u}\,\mathrm{d}A - \int_{\mathcal{B}}\mathbf{b}\cdot\delta\mathbf{u}\,\mathrm{d}V - \int_{\partial\mathcal{B}_N}\hat{\mathbf{t}}\cdot\delta\mathbf{u}\,\mathrm{d}A = 0\,, \tag{13}$$

where the fourth term in Eq. (13) is a stabilization term together with the stabilization parameter β which is constant on $\partial\mathcal{B}_D$. The idea is however, to keep the magnitude of the stabilization parameter β as low as possible to avoid an ill-conditioned discrete equation system.

In case of a linear problem Nitsche showed the existence of a certain minimum positive constant which ensures that the coefficient matrix of the discrete equation system is positive definite and the solution is approximated within optimal error bounds [19]. This constant could be related to β and was said to be dependent on the used basis polynomial and the chosen discretization of the solution space. The latter relates in meshfree methods to the covering of the problem domain $\mathcal{B}$ by the particle support zones which basically puts on geometric constraints on the intersections [11].

Applying this idea to solid mechanics we find, similar to the augmented Lagrangian method [23], that the material parameters strongly influence the determination of the stabilization parameter. Now it is desirable if a suitable value for the stabilization parameter β is computed automatically. To achieve this it was proposed to solve a general eigenvalue problem the following form,

$$\mathbf{Ax} = \lambda\mathbf{Bx}, \tag{14}$$

with the surface part of the stiffness matrix denoted by matrix $\mathbf{A}$ and the volume part by $\mathbf{B}$. The maximum eigenvalue was suggested to be taken as stabilization parameter [11]. Preliminary tests showed however, that this procedure leads to a magnitude of the stabilization parameter which is already at penalty levels. Thus, the stabilization term is dominating the problem formulation. Furthermore, in meshfree methods the boundary enforcement error is varying depending on the particle support. Therefore, it makes sense to consider the stabilization parameter as function of the coordinates charts θ^1 and θ^2 which describe the boundary $\partial\mathcal{B}_D$. We rewrite the modified variational principle Eq. (13) as follows

$$\delta\Pi(\mathbf{u}) = \int_{\mathcal{B}} \mathbf{S} : \delta\mathbf{E}\,\mathrm{d}V - \int_{\partial\mathcal{B}_D} \mathbf{FSn}\cdot\delta\mathbf{u}\,\mathrm{d}A - \int_{\partial\mathcal{B}_D} \delta(\mathbf{FSn})\cdot(\mathbf{u}-\hat{\mathbf{u}})\,\mathrm{d}A$$
$$+\int_{\partial\mathcal{B}_D}\beta(\theta^1,\theta^2,\hat{u}_i)\,(\mathbf{u}-\hat{\mathbf{u}})\cdot\delta\mathbf{u}\,\mathrm{d}A - \int_{\mathcal{B}}\mathbf{b}\cdot\delta\mathbf{u}\,\mathrm{d}V - \int_{\partial\mathcal{B}_N}\hat{\mathbf{t}}\cdot\delta\mathbf{u}\,\mathrm{d}A = 0\,. \tag{15}$$

In the discretized domain this means that the stabilization parameter is computed for each integration point individually and is not constant on $\partial\mathcal{B}$. Inspired by an iteration procedure applied to the augmented Lagrangian method [23] we are utilizing an iteration procedure to determine the minimum necessary penalty value at each integration point in order to ensure solution stability and a high convergence rate.

The idea is to run the problem first as geometrically linear one and to compare at each integration point the error in the essential boundary condition enforcement ϵ with a given error tolerance δ,

$$\epsilon(\theta^1,\theta^2,\hat{u}_i) = \left|\, u_i(\theta^1,\theta^2) - \hat{u}_i(\theta^1,\theta^2)\,\right| < \delta\,. \tag{16}$$

The value of this parameter δ is usually taken similarly to the limit of the convergence norm of the displacement field used for the Newton–Raphson method. The magnitude of the error in the boundary condition enforcement provides an indication of how much the constraint reaction resultant is too low. Depending on whether the error is higher or lower than the given error tolerance the stabilization parameter is increased or decreased correspondingly. Using these new adapted stabilization parameters and assigning to all particle parameter zero values the problem is then

solved again and the stabilization parameters are again modified if necessary. This process is repeated until the error tolerance is achieved at all integration points. It usually takes about five to ten iteration steps to determine a suitable stabilization parameter distribution. At the start of this procedure $\beta(\theta^1, \theta^2, h_i)$ is estimated for all integration points individually by the following expression,

$$\beta(\theta^1, \theta^2, \hat{u}_i) = \frac{\epsilon(\theta^1, \theta^2, \hat{u}_i)}{\delta}, \tag{17}$$

where ϵ is the boundary condition enforcement error evaluated after the first iteration step. During the iteration procedure $\beta(\theta^1, \theta^2, \hat{u}_i)$ is successively increased or decreased depending on the error of the boundary enforcement.

Note that in case of the augmented Lagrangian method the iteration procedure is undertaken with respect to the stabilization parameters as well as the Lagrange multipliers, but the modified variational principle Eq. (15) only requires the stabilization parameters to be obtained. That is the error in the essential boundary condition fulfillment is compensated by the stabilization term.

For more details on the iteration algorithm the reader is referred to Appendix A.

5. Numerical examples

5.1. Study on essential boundary condition enforcement

In the following our aim is to study the applicability of the proposed stabilized modified variational principle on two different examples. Three different cases are distinguished: Firstly, using the modified variational principle together with the iterative stabilization parameter determination algorithm Eq. (15), secondly, using this modified variational principle with a constant and uniform stabilization parameter $\beta \in \partial\mathcal{B}_D$ which is Eq. (13), and finally, applying instead of the modified variational principle the conventional penalty method to enforce the essential boundary conditions. That is, only the penalty term with a constant penalty parameter β is incorporated in the original variational formulation Eq. (12), but not the other boundary terms which led to the modified variational principle Eq. (13).

Furthermore, two different material laws are utilized. These are the linear Saint-Venant–Kirchhoff model with the material parameters *Young's modulus* E and *Poisson's ratio* ν and a non-linear statistically based model of hyperelasticity proposed by Arruda and Boyce [2] which involves as constitutive parameters the shear modulus C_R, the bulk modulus κ and parameter N. The constant N addresses the limited extensibility of the macromolecular network structure of the rubber material. The details of the model are presented in Appendix B.

Cantilever beam under pressure loading

The first study is a cantilever beam which is subjected to a constant pressure load on its top surface. It makes use of the *Saint-Venant–Kirchhoff* constitutive model and is illustrated in Fig. 1. The beam is modelled using 26 particles in longitudinal and only 2 in thickness direction. The stabilization parameters in the modified variational principle are kept uniform on $\partial\mathcal{B}_D$ and the results are compared with those achieved applying the penalty method instead. The boundary enforcement for different magnitudes of stabilization and penalizing is displayed in Fig. 2 and the

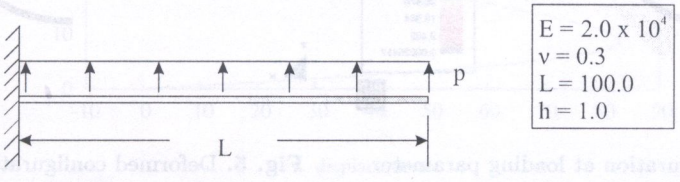

Fig. 1. Problem definition

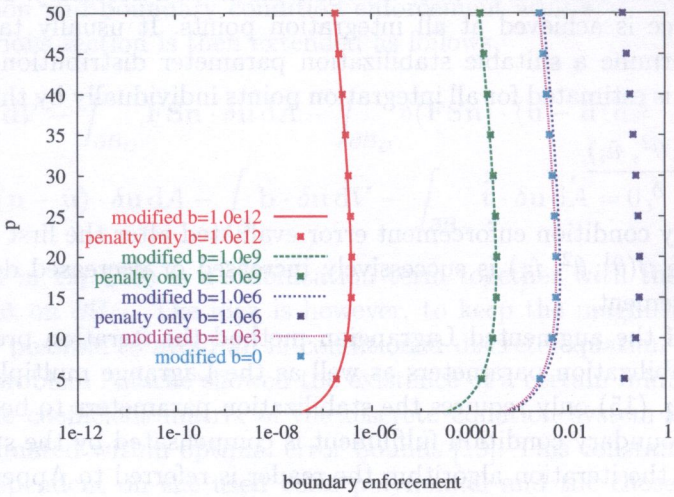

Fig. 2. Boundary enforcement

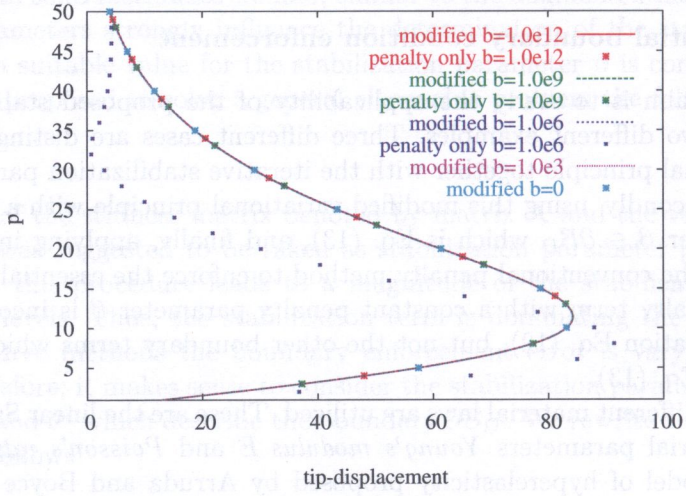

Fig. 3. Displacement diagram

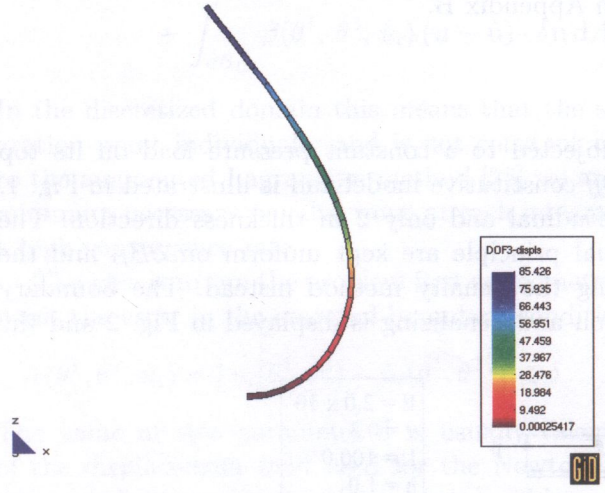

Fig. 4. Deformed configuration at loading parameter $p = 30$

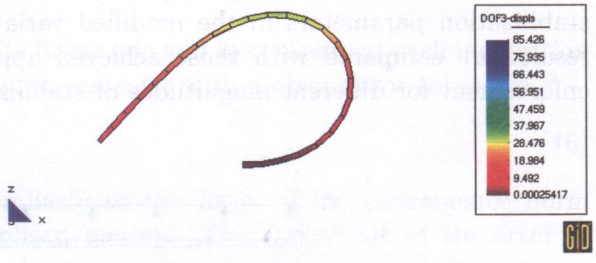

Fig. 5. Deformed configuration at loading parameter $p = 50$

corresponding tip deflection in Fig. 3. Note that the curves illustrating the tip deflection fall into one single line except for the one which represents the solution obtained using the penalty method with $\beta = 1.0 \times 10^6$ denoted by the dotted blue curve. We further find that the enforcement of the essential boundary conditions is best, if β is chosen to 1.0×10^{12}. The accuracy of our problem formulation is identical to the penalty method based formulation for parameters $\beta = 1.0 \times 10^{12}$ to $\beta = 1.0 \times 10^9$. The penalty method fails to provide meaningful results for penalty parameter values $\beta \leq 1.0 \times 10^6$. Using our proposed modified variational principle the stabilization parameter β can be chosen absolutely freely in order to achieve an accurate result for the tip deflection. Nevertheless, the accuracy of the boundary enforcement and the convergence rate become poorer for decreasing stabilization parameter values. In case of the modified variational formulation the lack of boundary approximation accuracy is for low values of the stabilization parameter quite significant, nonetheless we find good solutions for the tip deflection. The reason might be that the area having essential boundary conditions applied is minor compared to total surface of the problem domain. Moreover, there is no variation in the boundary approximation accuracy on all four affected particles and all integration points used for the surface integration of $\partial\mathcal{B}_D$.

The deformed configuration depicted in Figs. 4 and 5 are modelled with the modified variational principle setting $\beta(\theta^1, \theta^2, \hat{u}_i) = 0$ on $\partial\mathcal{B}_D$. Since the pressure acts during the entire simulation always perpendicular to the surface, the deformation process results in a kind of an ellipsoid.

Next, the above cantilever beam is again modelled with the same particle discretization but using the non-linear hyperelastic material law instead of the linear Saint-Venant–Kirchhoff and is depicted in Fig. 6.

Similar to the first study the stabilization term in the modified variational principle is not needed. It is therefore simulated with $\beta(\theta^1, \theta^2, \hat{u}_i) = 0$ on $\partial\mathcal{B}_D$. The displacement diagram for the cantilever beam's tip is shown in Fig. 7 and the final deformed configuration in Fig. 9. The use of the penalty method is again critical, because only with the knowledge of the solution the correct penalty parameter can be determined.

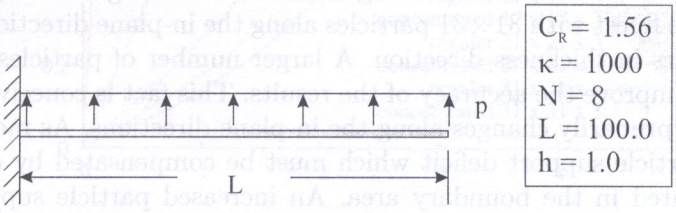

Fig. 6. Problem definition

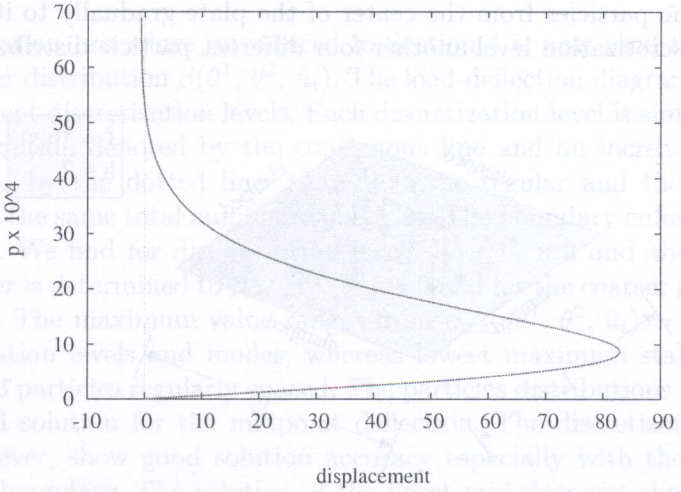

Fig. 7. Displacement diagram

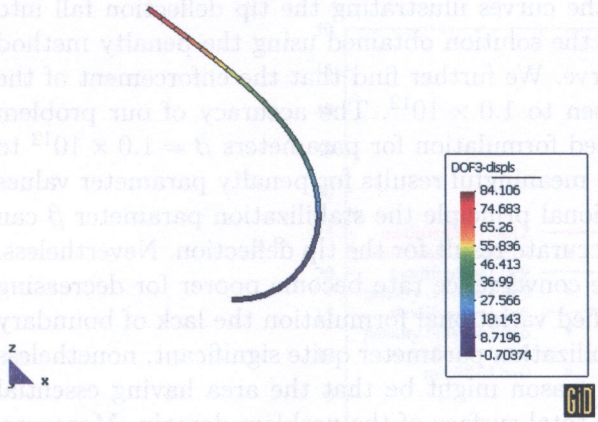

Fig. 8. Deformed configuration at loading parameter 13.5×10^4

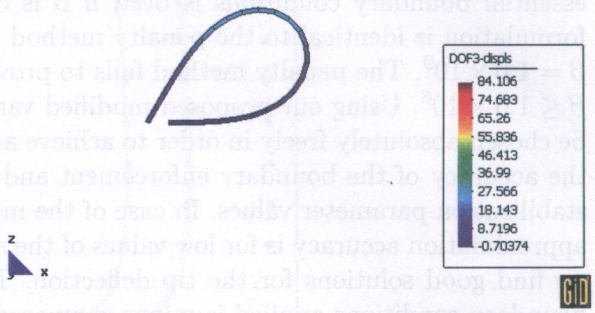

Fig. 9. Deformed configuration at loading parameter 69.0×10^4

Square sheet under dead loading

The next study's problem configuration is depicted in Fig. 10. It is a square sheet which is clamped at all four edges and subjected to a dead loading. It can be frequently found in literature. This problem is much more sensitive with respect to choice for the stabilization or penalty parameter than the cantilever beam presented in the previous paragraph. This is clear, as the analytical solution for cantilever beam's deflection only contains third order exponents of the longitudinal coordinate, whereas for the clamped plate's deflection fourth order exponents of the in-plane coordinates.

Considering that the approximation accuracy plays a crucial role especially on the boundary, different discretization levels are tested starting from the coarsest grid with 9×9, further 13×13, 17×17, 21×21 and the finest with 31×31 particles along the in-plane directions. Each configuration has three particle layers in thickness direction. A larger number of particles in thickness direction does not significantly improve the accuracy of the results. This fact is conceivable, as the solution of the displacement field primarily changes along the in-plane directions. As mentioned before we find on the boundary a particle support deficit which must be compensated by enlarging the influence zones of particles located in the boundary area. An increased particle support however means a decrease of approximation locality and thus accuracy which is crucial for the modified variational principle. In order to circumvent this dilemma it is also meaningful not only to analyze equally spaced particle distributions, but additionally grids that are denser towards the boundary. This is achieved by shifting the particles from the center of the plate gradually to its edges. Therefore we distinguish for each discretization level another four different particle distribution densities ranging

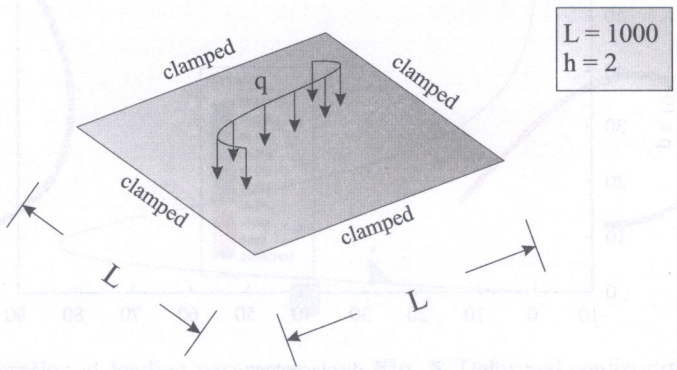

Fig. 10. Problem definition

from equally spaced to strongly concentrated on the boundaries. By concentrating the particles towards the plate's edges the boundary and the inner domain approximation accuracy is expected to be more in balance, what should improve the overall applicability of the proposed modified variational principle. It is important to stress that the particle density is continuously increased towards the boundary. Otherwise, there would be jumps in the particle density and the particle distribution would be too irregular resulting in a negative effect on the approximation accuracy.

At first, the Saint-Venant–Kirchhoff constitutive law is applied with the material parameters *Young's modulus* $E = 2.0 \times 10^4$ and *Poisson's ratio* $\nu = 0.3$. The use of the penalty method exhibits the general difficulty that various solutions can be obtained for penalty parameters ranging from $\beta = 1.0$ to 1.0×10^{12}. This means the problem behaves too soft or far too stiff. The correct result for the midpoint deflection however, can be found for $\beta \approx 1.0 \times 10^6$, whereas the boundary condition enforcement is always the best for $\beta = 1.0 \times 10^{12}$. It is therefore impossible to find out a suitable penalty parameter without the knowledge of the correct result.

The modified variational principle provides with $\beta(\theta^1, \theta^2, \hat{u}_i) = 0$ on $\partial\mathcal{B}_D$ for geometrically linear modelling a solution for the midpoint deflection which is the best achievable for each discretization level. The essential boundary condition enforcement however, is poor so that geometrically non-linear modelling fails for whatever particle distributions without utilizing the stabilization term.

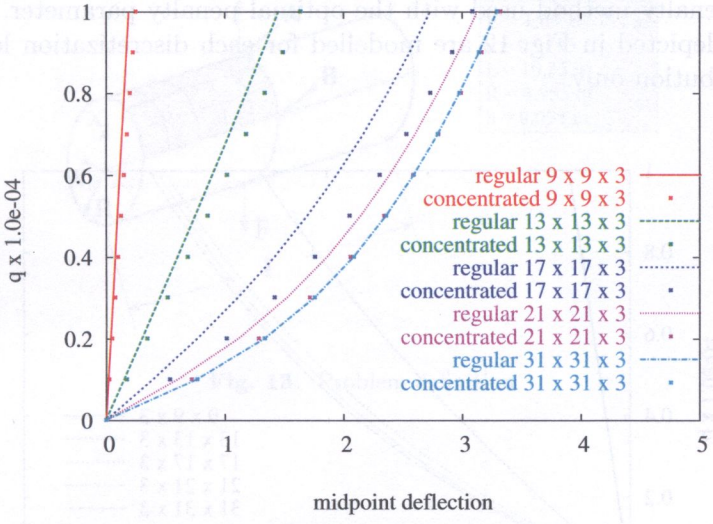

Fig. 11. Displacement diagram of the midpoint deflection — linear material

Therefore, the iteration procedure introduced in Section 4 is now used to determine a suitable stabilization parameter distribution $\beta(\theta^1, \theta^2, \hat{u}_i)$. The load-deflection diagrams illustrated in Fig. 11 are modelled for different discretization levels. Each discretization level is simulated with a regularly spaced particle distribution denoted by the continuous line and an increased particle density on the boundary denoted by the dotted line. Note that the regular and the concentrated particle distribution have each the same total number of particles. The boundary enforcement error tolerance is set $\delta = 1.0 \times 10^{-8}$. We find for discretization levels $17 \times 17 \times 3$ and above that the minimum stabilization parameter is determined to $\beta_{\min}(\theta^1, \theta^2) = 0$ and for the coarser grids it does not exceed $\beta(\theta^1, \theta^2, \hat{u}_i)_{\min} = 15$. The maximum value ranges from $\beta_{\max}(\theta^1, \theta^2, \hat{u}_i) = 5.0 \times 10^7 - 1.0 \times 10^{10}$ for different discretization levels and modes, whereas lowest maximum stabilization parameter is achieved for $31 \times 31 \times 3$ particles regularly spaced. The particles distributions $9 \times 9 \times 3$ and $13 \times 13 \times 3$ fail to provide a good solution for the midpoint deflection. The discretization levels $17 \times 17 \times 3$ and $21 \times 21 \times 3$ however, show good solution accuracy especially with the concentrated particle distribution near the boundary. The solution of the finest grid does not significantly change, if we apply higher particle density on the plate's edges.

In all cases the highest values for $\beta(\theta^1, \theta^2, \hat{u}_i)$ are always found at the clamped edges of the plate, whereas the lowest within the domain on the symmetry boundary. The minimum and maximum stabilization parameters can not be said to be significantly influenced by varying particle distribution. It seems that the constitutive law and the magnitude of its parameters have the main impact. This finding partly coincides with results of the next study, where the stiffness matrix norm is lower and correspondingly $\beta_{\max}(\theta^1, \theta^2, \hat{u}_i)$ has much lower values compared to this example.

In the next step the non-linear statistically based constitutive law is applied which involves as material parameters the shear modulus $C_R = 10 \times 10^3$, the bulk modulus $\kappa = 10.0 \times 10^7$ and parameter $N = 8$. These parameter are chosen in such way to provide a similar rigidity as we had for the Saint-Venant–Kirchhoff model. The boundary enforcement error tolerance is set $\delta = 1.0 \times 10^{-8}$. Compared to the previous study with the linear material law we find a substantially better boundary condition enforcement accuracy and consequently much lower values for the stabilization parameters $\beta_{\min}(\theta^1, \theta^2, \hat{u}_i) = 0$ and $\beta_{\max}(\theta^1, \theta^2, \hat{u}_i) = 6.0 \times 10^4$ are computed in order to achieve a stable and fast converging non-linear simulation. Especially the two highest discretization levels do not need the stabilization term at all. For particle discretization levels $17 \times 17 \times 3$ and above a higher particle density on the plate's edges significantly improves the boundary enforcement accuracy, but not the midpoint deflection. Apparently, the boundary approximation accuracy provided by a regular particle distribution is in case of the non-linear constitutive model already sufficient enough to achieve the best possible solution for given number of particles. The convergence rate is almost as high as having the penalty method used with the optimal penalty parameter. Therefore, the load-deflection diagrams depicted in Fig. 12 are modelled for each discretization level with a regularly spaced particle distribution only.

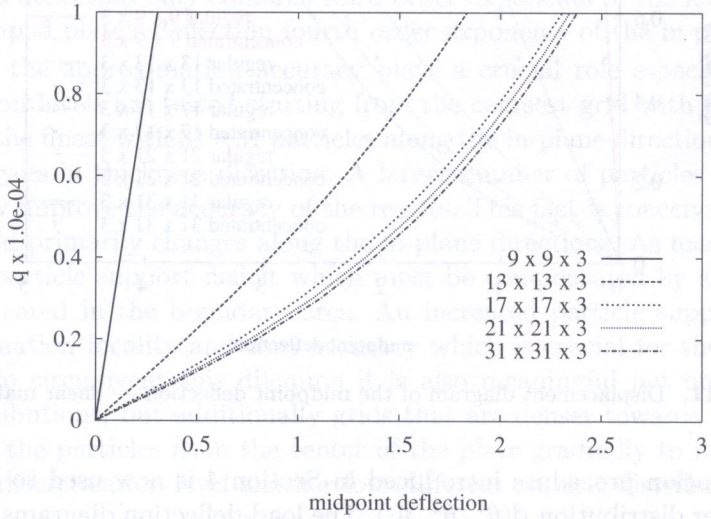

Fig. 12. Displacement diagram of the midpoint deflection — non-linear material

5.2. Shell deformation examples

After demonstrating the excellent applicability of the modified variational formulation Eq. (15) in the previous sub-section, three further examples are presented that feature large deformations of shells. The problem configurations of all examples are discretized by regularly spaced particle grids and the modified variational principle is applied using the iterative stabilization parameter computation algorithm to determine the stabilization parameter distribution $\beta(\theta^1, \theta^2, \hat{u}_i)$ on $\mathcal{B}$. The boundary enforcement error tolerance is set $\delta = 1.0 \times 10^{-8}$.

Pinched cylinder with free edges

This example is a classical one, a cylindrical shell is subjected to two vertically opposite point loads at its central points (point A) as depicted in Fig. 13. Assuming appropriate symmetry boundary conditions, the cylinder is modelled using one octant with 6 particles in longitudinal, 16 in radial, and 3 in thickness direction. The applied constitutive law is the Saint-Venant–Kirchhoff model. The displacement diagram in Fig. 14 is illustrated for point A and point B. The diagram shows that the deformation process is split into two parts. The first part is bending dominated which results in large deformations for small loading parameters. The second part is characterized by a steep slope. In Fig. 16, the final deformed configuration is displayed. It should be mentioned that this example has been considered by many authors using different shell finite elements. In fact, our numerical results are in good agreement with those reported in the literature. The iterative stabilization parameter determination provides values $\beta(\theta^1, \theta^2, \hat{u}_i) = 118.8$ to 6.1×10^{10}. Even if the solution exhibits a final boundary enforcement error $\epsilon = 1.3 \times 10^{-4}$ the modelling is stable and converges at high rates.

The remaining two applications make use of the non-linear statistically based model involving as constitutive parameters the shear modulus C_R, the bulk modulus κ and the parameter N.

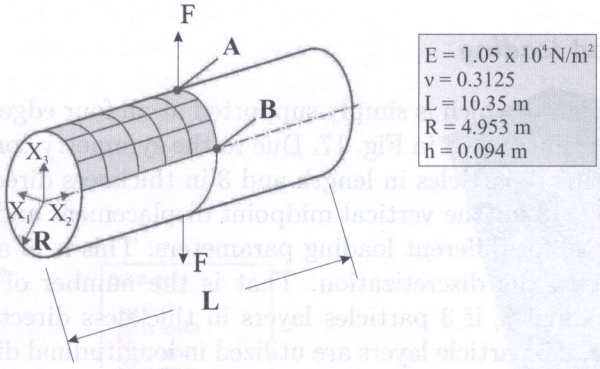

Fig. 13. Problem definition

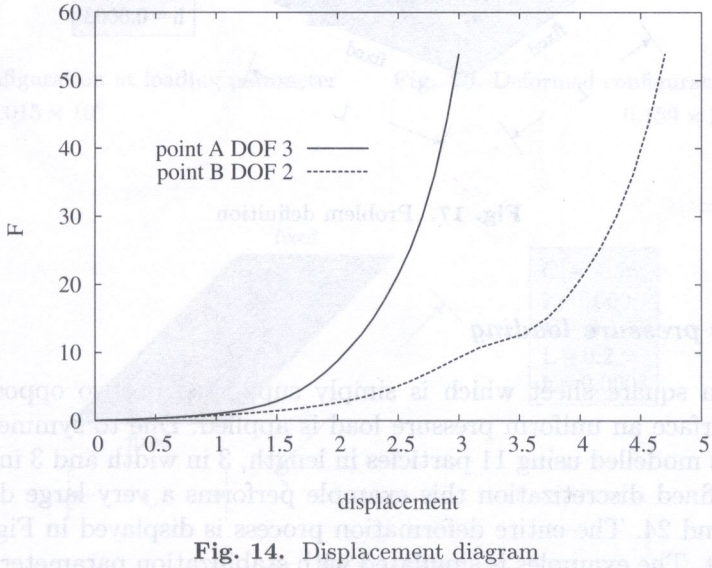

Fig. 14. Displacement diagram

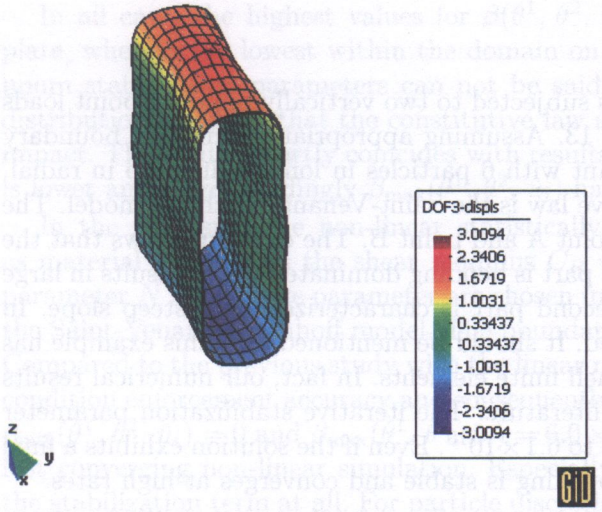

Fig. 15. Deformed configuration at loading parameter 8.78

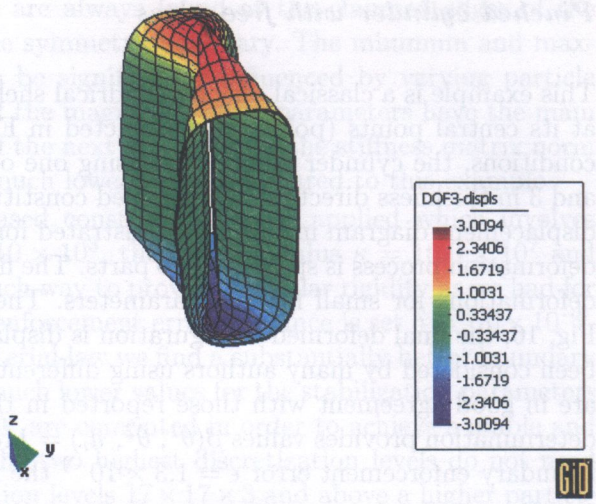

Fig. 16. Deformed configuration at loading parameter 53.95

Square sheet under dead loading

The following example is a sheet which is simply supported at all four edges and subjected to a dead loading on its top surface as illustrated in Fig. 17. Due to the symmetry conditions, only one quarter of the sheet is modelled using 6 particles in length and 3 in thickness direction. The load-deflection diagram is presented in Fig. 18 for the vertical midpoint displacement and deformed configurations are shown in Figs. 19 and 20 for different loading parameters. This is of all our examples the most sensitive one with respect to the discretization. That is the number of particle layers in length direction is limited to maximal 7, if 3 particles layers in thickness direction are chosen. The best results we can find however, if 5 particle layers are utilized in longitudinal direction. The stabilization parameters in this particular examples is determined to $\beta(\theta^1, \theta^2, \hat{u}_i) = 1.4 \times 10^3$ to 3.5×10^7.

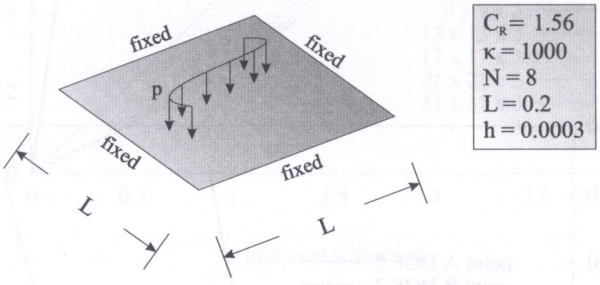

Fig. 17. Problem definition

Square sheet under pressure loading

Our last example is a square sheet which is simply supported at two opposite edges shown in Fig. 21. On its top surface an uniform pressure load is applied. Due to symmetry conditions, only one half of the sheet is modelled using 11 particles in length, 3 in width and 3 in thickness direction. Despite a not very refined discretization this example performs a very large deformation which is depicted in Figs. 23 and 24. The entire deformation process is displayed in Fig. 22 for the vertical midpoint displacement. The examples is simulated with stabilization parameters $\beta(\theta^1, \theta^2, \hat{u}_i) = 0.0$ to 7.0×10^{-5}.

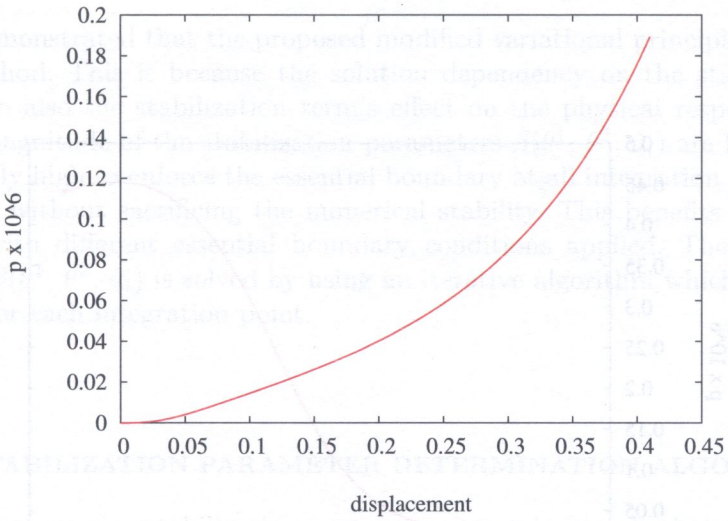

Fig. 18. Displacement diagram

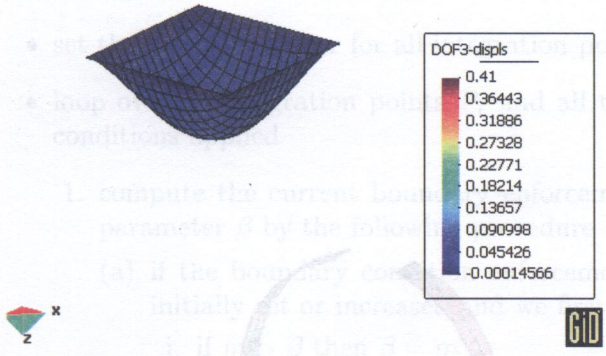

Fig. 19. Deformed configuration at loading parameter 0.015×10^6

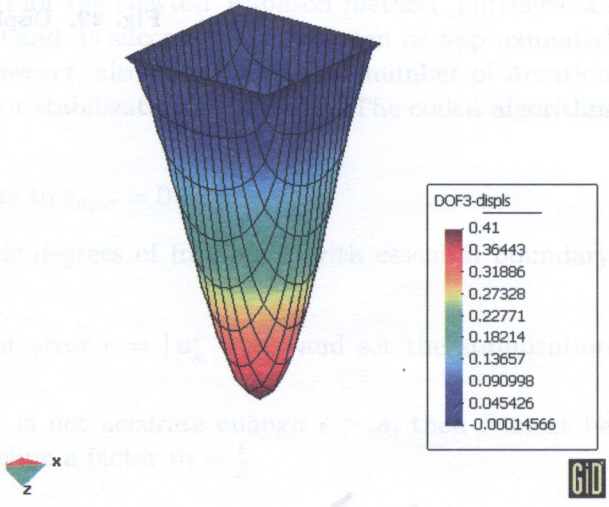

Fig. 20. Deformed configuration at loading parameter 0.189×10^6

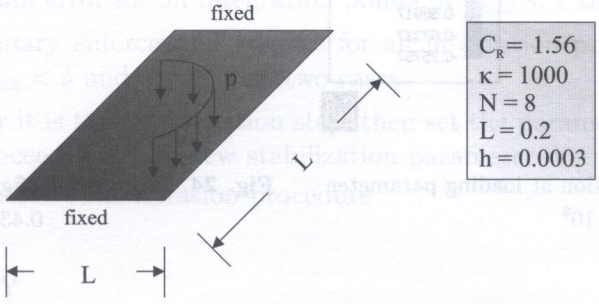

Fig. 21. Problem definition

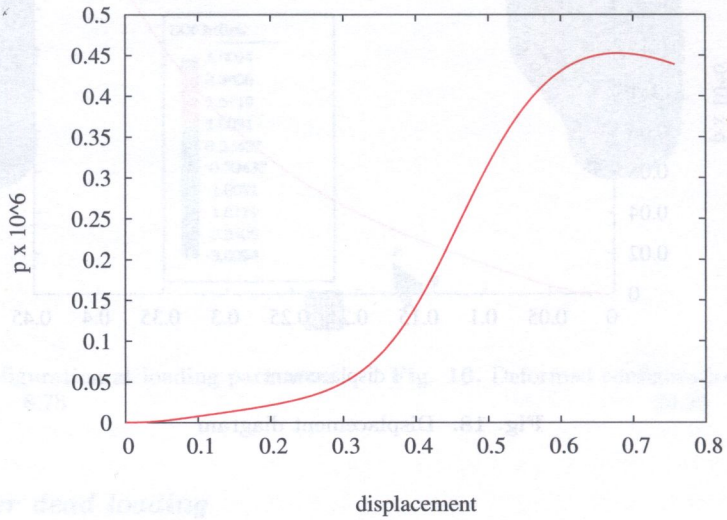

Fig. 22. Displacement diagram

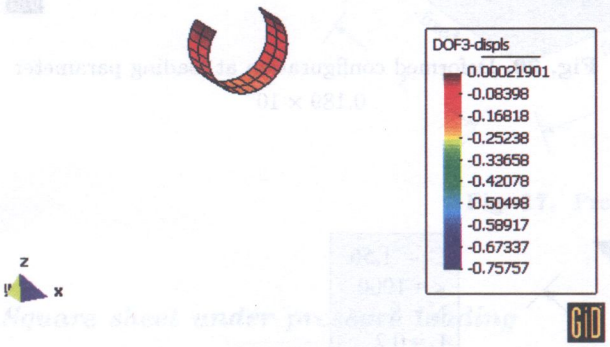

Fig. 23. Deformed configuration at loading parameter 0.008×10^6

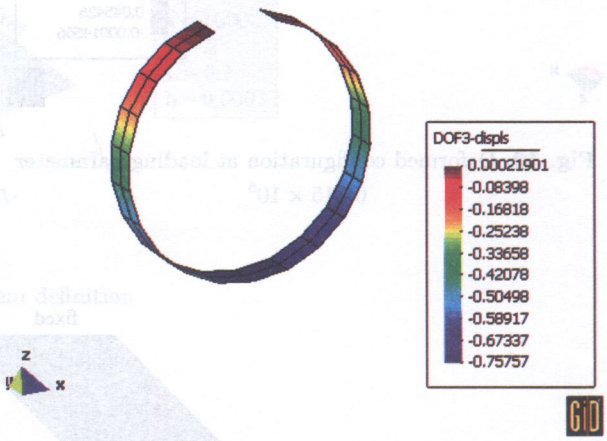

Fig. 24. Deformed configuration at loading parameter 0.439×10^6

6. Conclusion

In this paper we demonstrated that the proposed modified variational principle is a real alternative to the penalty method. This is because the solution dependency on the stabilization parameter is minimized and so also the stabilization term's effect on the physical response of the problem. Furthermore, the magnitude of the stabilization parameters $\beta(\theta^1, \theta^2, \hat{u}_i)$ are kept at relatively low levels, but sufficiently high to enforce the essential boundary at all integration points within a given error tolerance and without sacrificing the numerical stability. This benefits a high adaptivity to various problems with different essential boundary conditions applied. The difficulty of finding suitable values for $\beta(\theta^1, \theta^2, \hat{u}_i)$ is solved by using an iterative algorithm which allows to determine them individually for each integration point.

Appendix

A. Iterative stabilization parameter determination algorithm

The basic idea of the iterative stabilization parameter determination is that the parameters β are individually assigned to each numerical integration point and the final configuration ensures that at each integration point a minimum value of essential boundary condition enforcement δ is given. Parameter δ is a constant value applied to the entire problem domain. As already mentioned δ can be related to the displacement convergence norm used for the Newton–Raphson method. Furthermore the initial setting of the stabilization parameters β and its successive increase can be approximated by Eq. (17). The objective of this algorithm is however, also to minimize the number of iteration steps needed to computed a suitable distribution for stabilization parameters. The coded algorithm used for this work looks like follows:

- set the maximum error for all integration points to $\epsilon_{\max} = 0$
- loop over all integration points P_I and all their degrees of freedom k with essential boundary conditions applied
  1. compute the current boundary enforcement error $\epsilon = |u_k^I - \hat{u}_k^I|$ and set the stabilization parameter β by the following procedure
     (a) if the boundary condition enforcement is not accurate enough $\epsilon > \delta$, then β must be initially set or increased and we first define a factor $m = \frac{\epsilon}{\delta}$
        i. if $m > \beta$ then $\beta = m$
        ii. else if $m < 2.0$ then $\beta = \beta * 2.0$
        iii. else $\beta = \beta * m$
     (b) else if boundary condition enforcement is more accurate then required $\epsilon < \delta * 10$ then gradually reduced the stabilization parameter by $\beta = \beta/2$
  2. adjust the maximum error for all integration points: if $\epsilon_{\max} < \epsilon$ then $\epsilon_{\max} = \epsilon$
  3. check, if the boundary enforcement error is for all integration points lower than the given error tolerance $\epsilon_{\max} < \delta$ and distinguish two cases
     (a) if $\epsilon_{\max} > \frac{\delta}{10}$ or it is the first iteration step, then set the parameter of all particles to zero values and proceed with the new stabilization parameter distribution at 2.
     (b) otherwise terminate the iteration procedure

B. Hyper-elasticity

In order to simulate large elastic strains in rubber-like structures the neo-Hookean law was and is one of the simplest constitutive laws one may deal with. The Mooney–Rivlin law was an improvement

of this in terms of accuracy. In 1984 Ogden [20] introduced a far more accurate model, which was dependent on the eigenvalues of the stretch tensor, what made however the calculation of the tangent matrix extremely costly. All those models incorporated material constants, which had to be determined by experiments. Though, because the experimental data are directly related to standard tests, such as uni-axial stretch, bi-axial stretch and shear, the material behaviour might not be copied for any arbitrary loading or geometry configuration.

Contrarily, the statistically-based constitutive model proposed by Arruda and Boyce [2] assumed for the rubber material a macromolecular network structure consisting of eight chains and addresses also their non-Gaussian behaviour. The constitutive formulation involved only three constants: a shear modulus C_R, a bulk modulus κ and a parameter N, which addressed to limited extensibility of the network. Each of these parameters represented a physical property of the material and are not just experimental data.

Sansour *et al.* formulated a corresponding constitutive law and so also the stored energy function as a functional of the invariants of the right Cauchy–Green tensor [22]. The dependency on the right Cauchy–Green tensor provided the benefits that the computation of the derivatives was not complicated and also anisotropic material, it was said, could be dealt with. In the following a brief overview of this approach is given. Let us define first the invariants of the right Cauchy–Green strain tensor $\mathbf{C}$ as

$$I_1 = \operatorname{tr} \mathbf{C}, \qquad I_2 = \frac{1}{2}\left[(\operatorname{tr} \mathbf{C})^2 - \operatorname{tr} \mathbf{C}^2\right], \qquad I_3 = \det \mathbf{C}\,. \tag{B1}$$

Also a pair of modified invariants shall be taken into account,

$$\bar{I}_1 = \frac{I_1}{I_3^{\frac{1}{3}}}, \qquad \bar{I}_2 = \frac{I_2}{I_3^{\frac{2}{3}}}\,. \tag{B2}$$

Considering the material to be characterized by the volumetric–isochoric split, Anand proposed [1] the energy storage function in compressible form as

$$W = W^{\text{iso}} + W^{\text{vol}} \tag{B3}$$

with

$$W^{\text{iso}} = C_R \left[\frac{1}{2}(\bar{I}_1 - 3) + \frac{1}{20N}(\bar{I}_1{}^2 - 9) + \frac{11}{1050N^2}(\bar{I}_1{}^3 - 27) + \right.$$
$$\left. + \frac{19}{7000N^3}(\bar{I}_1{}^4 - 81) + \frac{519}{673750N^4}(\bar{I}_1{}^5 - 243) + \cdots\right], \tag{B4}$$

$$W^{\text{vol}} = \frac{1}{2}\kappa(\ln \sqrt{I_3})^2. \tag{B5}$$

Now is the second Piola–Kirchhoff stress tensor $\mathbf{S}$ defined as

$$\mathbf{S} = 2\frac{\partial W}{\partial \mathbf{C}} = a_1\,\mathbf{1} + a_2\,\mathbf{C} + a_3\,\mathbf{C}^{-1} \tag{B6}$$

with

$$a_1 = 2C_R\left(\frac{1}{2} + \frac{1}{10N}\bar{I}_1 + \frac{11}{350N^2}\bar{I}_1{}^2 + \frac{19}{1750N^3}\bar{I}_1{}^3 + \frac{519}{134750N^4}\bar{I}_1{}^4 + \ldots\right) I_3^{-\frac{1}{3}},$$

$$a_2 = 0\,,$$

$$a_3 = -\frac{2}{3}C_R\left(\frac{1}{2} + \frac{1}{10N}\bar{I}_1 + \frac{11}{350N^2}\bar{I}_1{}^2 + \frac{19}{1750N^3}\bar{I}_1{}^3 + \frac{519}{134750N^4}\bar{I}_1{}^4 + \cdots\right)\bar{I}_1 + \kappa \ln \sqrt{I_3}\,,$$

and if one takes into account that

$$\frac{\partial I_1}{\partial \mathbf{C}} = \mathbf{1}, \qquad \frac{\partial I_2}{\partial \mathbf{C}} = I_1\,\mathbf{1} - \mathbf{C}, \qquad \frac{\partial I_3}{\partial \mathbf{C}} = I_3\mathbf{C}^{-1}\,. \tag{B7}$$

Finally the second order derivative of the energy storage function with respect to $\mathbf{C}$ provides the constitutive tensor $\mathcal{C}$,

$$\mathcal{C} = 2\frac{\partial^2 W}{\partial \mathbf{C}\partial \mathbf{C}} = = 2\left[b_1\delta_{ij}\delta_{rs} + b_2\left((\mathbf{C}^{-1})_{ij}\delta_{rs} + \delta_{ij}(\mathbf{C}^{-1})_{rs}\right) + \right.$$
$$\left. + (b_3+b_4)(\mathbf{C}^{-1})_{ij}(\mathbf{C}^{-1})_{rs} - (b_5+b_6)(\mathbf{C}^{-1})_{ir}(\mathbf{C}^{-1})_{sj}\right], \tag{B8}$$

with the following coefficients,

$$b_1 = C_R I_3^{-\frac{1}{3}}\left[\frac{1}{10N} + \frac{11}{175N^2}\bar{I}_1 + \frac{57}{1750N^3}\bar{I}_1{}^2 + \frac{1038}{67375N^4}\bar{I}_1{}^3 + \frac{59991}{8758750N^5}\bar{I}_1{}^4 + \cdots\right],$$

$$b_2 = -\frac{1}{3}C_R I_3^{-\frac{1}{3}}\left[\frac{1}{2} + \frac{1}{5N}\bar{I}_1 + \frac{33}{350N^2}\bar{I}_1{}^2 + \frac{38}{875N^3}\bar{I}_1{}^3 + \frac{519}{26950N^4}\bar{I}_1{}^4 + \cdots\right],$$

$$b_3 = \frac{1}{9}C_R\left[\frac{1}{2}\bar{I}_1 + \frac{1}{5N}\bar{I}_1{}^2 + \frac{33}{350N^2}\bar{I}_1{}^3 + \frac{38}{875N^3}\bar{I}_1{}^4 + \frac{519}{26950N^4}\bar{I}_1{}^5 + \cdots\right],$$

$$b_4 = \frac{\kappa}{4},$$

$$b_5 = -\frac{1}{3}C_R\bar{I}_1\left[\frac{1}{2} + \frac{1}{10N}\bar{I}_1 + \frac{11}{350N^2}\bar{I}_1{}^2 + \frac{19}{1750N^3}\bar{I}_1{}^3 + \frac{519}{134750N^4}\bar{I}_1{}^4 + \cdots\right],$$

$$b_6 = \frac{1}{2}\kappa\ln\sqrt{I_3}.$$

References

[1] L. Anand. A constitutive model for compressible elastomeric solids. *Computational Mechanics*, **18**: 339–355, 1996.

[2] E.M. Arruda, M.C. Boyce. A three-dimensional constitutive model for the large stretch behaviour of rubber elastic materials. *Journal of the Mechanics and Physics of Solids*, **41**: 389–412, 1993.

[3] T. Belytschko, L. Gu, Y.Y. Lu. Fracture and crack growth by element-free Galerkin methods. *Modelling and Simulation in Materials Science and Engineering*, **2**: 519–534, 1994.

[4] T. Belytschko, Y.Y. Lu, L. Gu. Element free Galerkin methods. *International Journal for Numerical Methods in Engineering*, **37**: 229–256, 1994.

[5] P. Breitkopf, A. Rassineux, P. Villon. An introduction to moving least squares meshfree methods. *Revue Européenne des Eléments Finis*, **11**(7–8): 825–868, 2002.

[6] J.-S. Chen, C. Pan, C.-T. Wu. A large deformation analysis of rubber based on a reproducing kernel particle method. *Computational Mechanics*, **19**: 211–227, 1997.

[7] J.Y. Cho, Y.M. Song, Y.H. Choi. Boundary locking induced by penalty enforcement of essential boundary conditions in mesh-free methods. *Computer Methods in Applied Mechanics and Engineering*, **197**: 1167–1183, 2008.

[8] S. De and K.-J. Bathe. The method of finite spheres. *Computational Mechanics*, **25**: 329–345, 2000.

[9] J. Dolbow, T. Belytschko. Numerical integration of Galerkin weak form in meshfree methods. *Computational Mechanics*, **23**(3): 219–230, 1999.

[10] C.A. Duarte, J.T. Oden. Hp clouds — a hp meshless method, *Numerical Methods Partial Differential Equations*, **12**: 673–705, 1996.

[11] M. Griebel, M.A. Schweitzer. A particle-partition of unity method – Part V: Boundary conditions. In: S. Hildebrandt, H. Karcher, eds., *Geometric Analysis and Nonlinear Partial Differential Equations*, pp. 517–540. Springer, 2002.

[12] R. Hestenes. Multiplier and gradient methods. *Journal of Optimization Theory and Applications*, **4**: 303–320, 1969.

[13] P. Lancaster, K. Salkauskas. Surface generated by moving least square methods. *Mathematics of Computations*, **37**(155): 141–158, 1981.

[14] W.K. Liu, Y. Chen. Wavelet and multiple scale reproducing kernel methods. *Journal of Numerical Methods in Fluids*, **21**: 901–931, 1995.

[15] G.R. Liu, X.L. Chen. A mesh-free method for static and free vibration analysis of thin plates of complicated shape. *Journal of Sound and Vibration*, **241**(5): 839–855, 2001.

[16] Y.Y. Lu, T. Belytschko, L. Gu. A new implementation of the element free Galerkin method. *Computer Methods In Applied Mechanics And Engineering*, **113**: 397–414, 1994.

[17] J.M. Melenk, I. Babuska. The partition of unity method: Basic theory and applications. *International Journal for Numerical Methods in Engineering*, **40**: 727–758, 1997.

[18] B. Nayroles, G. Touzot, P. Villon. Generalizing the finite element method: Diffuse approximation and diffuse elements. *Computational Mechanics*, **10**: 307–318, 1992.

[19] J. Nitsche. Über ein Variationsprinzip zur Lösung von Dirichlet-Problemen bei Verwendung von Teilräumen, die keinen Randbedingungen unterworfen sind. *Abh. Math. Sem. Univ. Hamburg*, **36**: 9–15, 1970–1971.

[20] R.W. Ogden. *Non-linear Elastic Deformation*, Ellis Horwood, Chichester, 1984.

[21] J.D. Powell. A method for non-linear constraint in optimization problems. In: R. Fletcher, ed., *Optimization*, Academic Press, London, 283–298, 1969.

[22] C. Sansour, S. Feih, W. Wagner. On the performance of enhanced strain finite elements in large strain deformations of elastic shells. *International Journal for Computer-Aided Engineering and Software*, **20**(7): 875–895, 2003.

[23] G. Ventura. An augmented Lagrangian approach to essential boundary conditions in meshless methods. *International Journal For Numerical Methods In Engineering*, **53**: 825–842, 2002.

[24] G.J. Wagner, W.K. Liu. Application of essential boundary conditions in mesh-free methods: a corrected collocation method. *International Journal for Numerical Methods in Engineering*, **47**(2): 1367–1379, 2000.